AIChE WILEY InterScience DISCOVER SOMETHING GREAT



# Structure, Interaction and Property of Amino-Functionalized Imidazolium ILs by Molecular Dynamics Simulation and Ab Initio Calculation

**Guangren Yu**
State Key Laboratory of Multiphase Complex Systems, Institute of Process Engineering, Chinese Academy of Sciences, 100080 Beijing, China and College of Chemical Engineering, Beijing University of Chemical Technology, 100029 Beijing, China

**Suojiang Zhang, Guohui Zhou, and Xiaomin Liu**
State Key Laboratory of Multiphase Complex Systems, Institute of Process Engineering, Chinese Academy of Sciences, 100080 Beijing, China

**Xiaochun Chen**
College of Chemical Engineering, Beijing University of Chemical Technology, 100029 Beijing, China

*DOI 10.1002/aic.11339*
*Published online October 22, 2007 in Wiley InterScience (www.interscience.wiley.com).*

*Imidazolium ionic liquids (ILs) can be functionalized by introducing —$NH_2$, which were found to be excellent solvents for $CO_2$ capture and electrophile separation, however, some disadvantages, e.g., the relatively high viscosities, limit their eventual large-scale applications. To understand the influences of amino addition on their properties and promote their applications, the microstructure and interionic interaction in two selected amino-functionalized imidazolium ILs, 1-aminoethyl-3-methylimidazolium hexafluorophosphate and 1-aminopropyl-3-butylimidazolium tetrafluoroborate, are studied both for bulk liquid by using molecular dynamics simulations and for isolated ion pair by using ab initio calculations. It is found that the amino addition does not remarkably affect the organization of anions around C2-site, C4-site, and C5-site on imidazolium ring, while it participates in the cation–anion interaction as a new strong site where anions strongly organize around —$NH_2$ and form strong ion-type hydrogen bonds. The condensed phase simulations indicate that their ionic self-diffusion coefficients are on the order of $10^{-13}$ $m^2$ $s^{-1}$ at room temperature, roughly 2 order of magnitude lower than that of conventional imidazolium ILs without —$NH_2$; the isolated ion pair calculations show that such terminal amino-associated interaction reduces the flexibility of alkyl side chains and increases the cation–anion interaction; and these results are qualitatively consistent with their higher experimental viscosities.* © 2007 American Institute of Chemical Engineers *AIChE J,* 53: 3210–3221, 2007

This article contains Supplementary Material available via the Internet at http://www.interscience.wiley.com/jpages/0001-1541/suppmat.

Correspondence concerning this article should be addressed to S. Zhang at sjzhang@home.ipe.ac.cn and X. Chen at chenxc@mail.buct.edu.cn.

*Keywords: ionic liquids, molecular dynamics simulation, ab initio calculation, structure, interaction, viscosity*

## Introduction

The use of volatile organic solvents has brought serious environmental problems. There is a strong driving force to seek new alternatives. In the last 10 years, a new class of compounds, ionic liquids (ILs), have emerged and attracted increasing interests.[1–9] ILs are organic salts composed entirely of organic cations and inorganic/organic anions, while different from traditional high-temperature molten salts, e.g., NaCl, they are generally liquids at or below room temperature. They have negligible vapor pressure, and thus fugitive emissions in engineering applications will be significantly lower than those for conventional volatile organic solvents. Therefore, ILs has been proposed as "green solvents" or environmentally friendly solvents. One typical potential application of ILs is capturing $CO_2$ from nature gas and fuel gas where $CO_2$ is contaminant and atmosphere pollutant, respectively. Comparing with the traditional alkanolamine solutions process where the concurrent loss of volatile amines and the uptake of water into the gas stream cause intensive energy consumption, cost increase, and corrosion, ILs are preferable potential alternatives for their nonvolatility. Recent studies showed that imidazolium ILs have remarkable absorption capacities,[10–26] especially at relatively high pressures, e.g., the $CO_2$ solubility is on the order of 50 mol % at 5 MPa.[10] However, their absorption capabilities are poor at lower pressures,[11,15,17,21,25] e.g., about 0.02 mol $CO_2$/mol IL at atmospheric pressure and room temperature. To this regard, functional amino group was introduced to the alkyl side chain terminal of imidazolium ILs to tailor their performances, e.g., 1-(3-aminoethyl)-3-methylimidazolium hexafluorophosphate ([aemim][$PF_6$]) and 1-(3-aminopropyl)-3-butylimidazolium tetrafluoroborate ([apbim][$BF_4$]), Scheme 1.[27,28] The introduction of $-NH_2$ significantly enhances the absorption capabilities, e.g., at room temperature and atmospheric pressure 1 mol [apbim][$BF_4$] can absorb 0.5 mol $CO_2$,[28] which is about a few hundred times than that of conventional imidazolium ILs, such as [bmim][$PF_6$] and [bmim][$BF_4$], where [bmim] is 1-*n*-butyl-3-methylimidazolium. In addition, they also presented good performances in solution-phase parallel synthesis as electrophile scavenger[27] and in Knoevenagel reaction as catalyst.[29] However, as has been demonstrated, some undesirable properties, such as the high viscosities (e.g., the viscosity of [aemim][$PF_6$] is about 2 order of magnitude higher than that of conventional imidazolium ILs.[27]), may limit their eventual large-scale applications in industry.

A fundamental understanding of microstructure and interionic interaction in ILs is very valuable and necessary for understanding their properties, and further for rationalizing their designs. Molecular dynamics (MD) simulations have been used to study the microstructure of imidazolium ILs and predict their thermodynamic or dynamic properties.[30–45] It has been concluded that their liquid phases are strongly organized through widely existing interionic hydrogen bonds and electrostatic interaction; anions prefer to organize around C2-site on imidazolium ring and form strong hydrogen bonds with C2—H, then followed by C4—/C5—sites, and have a weak interaction with alkyl side chains; such strong interionic interaction is responsible for the long-range ordering in liquid, much higher vaporization heat and cohesive energy density that is consistent with their nonvolatile nature, and much lower ionic self-diffusion coefficients (e.g., the predicted ionic self-diffusion coefficients of imidazolium hexafluorophosphate and tetrafluoroborate ILs are around on the order of $10^{-11}$ $m^2$ $s^{-1}$ at room temperature,[32,33,36,45] which is about 2 order of magnitude lower than that of conventional molecule solvents, e.g., water is $2.3 \times 10^{-9}$ $m^2$ $s^{-1}$ at 298 K and 1 atm[46]). The local interaction on individual ions within imidazolium ILs can better be understood by investigating an isolated ion pair from ab initio calculations, which includes the geometries (cation–anion interaction site, hydrogen bond), electronic properties (charge, electron density, molecular orbital), cation–anion interaction energy, and thermodynamic properties in ideal gas state.[47–58] Such ion pair calculations have been employed to interpret their volatility, melting points, water solubility, chemical reactivity, and so on.[50,53,55,57] However, most of these studies are limited into the conventional imidazolium ILs.

With regard to the effects of microstructure and interionic interaction on the viscosity, there have been some intuitive understandings, such as the flexibility of alkyl side chains,[59–61] the geometric symmetry of and charge distribution on ions,[62,63] and the interionic hydrogen bonding, van der Waals, coulombic electrostatic interaction.[59,61,62,64,65] Our recent studies showed that the interionic interaction, such as hydrogen bonds, has an important effect on the liquid organization and viscosity, both from MD simulations[66–68] and ab initio calculations.[69] The influences of ionic structure and hydrogen bonding interaction on the reactivity of $-NH_2$ towards $CO_2$ have been investigated for such amino-functionalized imidazolium ILs by us.[58] In this work, in order to understand the influences of amino addition on the microstructure, interionic interaction, and properties, MD simulations, and ab initio calculations are performed for [aemim][$PF_6$] and [apbim][$BF_4$] to investigate the bulk liquids (including density, energy composition, volume expansivity, ionic organization, hydrogen bond, self-diffusion coefficient) and isolated ion pairs

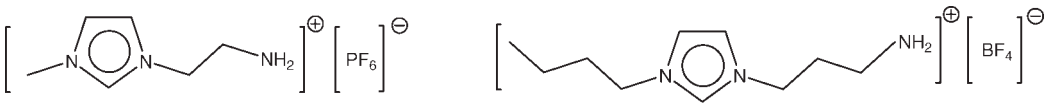


[aemim][$PF_6$] [apbim][$BF_4$]

**Scheme 1. Amino-functionalized Imidazolium ILs.**

**Table 1. Properties of Amino-Functionalized Imidazolium ILs, Calculated from Condensed Phase Molecular Dynamics Simulations**

| ILs | Temp. (K) | $U^{int}$ (kJ mol$^{-1}$) | $\Delta H^{vap}$ (kJ mol$^{-1}$) | $V_m$ (cm$^3$ mol$^{-1}$) | $c$ (J cm$^{-3}$) | Dens. (g cm$^{-3}$) | $D$ ($10^{-13}$ m$^2$ s$^{-1}$) | |
|---|---|---|---|---|---|---|---|---|
| | | | | | | | Cation | Anion |
| [aemim][$PF_6$] | 298.15 | −523.1 ± 1.3 | 123.3 | 176.0 | 686.4 | 1.540 ± 0.008 | 7.9 | 3.3 |
| | 333.15 | −524.3 ± 1.4 | 124.8 | 178.6 | 683.1 | 1.517 ± 0.008 | 43.4 | 15.5 |
| | 368.15 | −520.4 ± 1.5 | 121.2 | 181.7 | 650.0 | 1.492 ± 0.012 | 70.7 | 53.7 |
| [apbim][$BF_4$] | 298.15 | −540.4 ± 1.1 | 107.9 | 223.5 | 471.6 | 1.203 ± 0.009 | 9.0 | 7.3 |
| | 333.15 | −537.2 ± 1.2 | 105.0 | 228.7 | 446.9 | 1.176 ± 0.008 | 39.5 | 23.1 |
| | 368.15 | −528.6 ± 1.3 | 96.7 | 233.2 | 401.4 | 1.153 ± 0.009 | 173.1 | 131.1 |

(including cation–anion interaction pattern, interaction energy, hydrogen bond, the flexibility of side chain rotation), respectively.

## Computational Methods

### *MD simulation*

MD simulations for the bulk liquids were performed with MDynaMix.[70] The double time-step algorithm[71] was adopted, with long and short time steps of 2 and 0.2 fs, respectively. Ewald summation method[72] was used to treat the long-range electrostatic interaction, in which the short-range and long-range parts were cut off at a radius of 15 Å and a half-length of simulation box, respectively. The Lennard-Jones force was cut off at a radius of 15 Å. Each simulation system consists of 192 ion pairs. A typical simulation process is illustrated as follows. In *NVE* ensemble, a starting simulation is executed from an FCC lattice at a very low density and high temperature, typically 0.1 g cm$^{-3}$ and 700 K. After a relaxation for a few MD steps (around 20 ps) to reduce the possible overlapping in the initial configuration, the simulation is transferred into Nosé-Hoover *NPT* ensemble[73] to be performed with coupling constants 700 and 80 fs. Descending from 700 K to the sampling temperature, e.g., 298.15 K, a series of *NPT* simulations are performed with an equal interval of 50 K, each temperature point being lasted for 20 ps. At the sampling temperature point, it is equilibrated for at least 2 ns, then the production phase is lasted for 5 ns.

### *Ab initio calculation*

All the calculations were performed with GAUSSIAN 03.[74] The ab initio method of frozen-core second-order perturbation approximation Møller-Plesset (MP2)[75,76] and the density functional theory method of the well-established Becke's three-parameter hybrid functional[77] with the correlation functional of Lee et al.[78] (B3LYP) were used, combined with 6-31G* basis set, of which the abilities to calculate the structure and energy of ILs ion pair have been widely demonstrated.[47–58] Each optimized structure was checked to be a true minimum and not a saddle point through frequency calculation.

## Results and Discussion

### *MD simulation of bulk liquids*

*Force Field Development.* The force field in AMBER framework was adopted in this work, and their abilities to simulate imidazolium ILs have been widely demonstrated.[33–36,41,43,44,66–68,79] Because of the addition of amino group, some new force field parameters need to be regressed. The development details and complete listing of force field parameters are provided in the Supporting Information.

*Simulation Results*

*Liquid density.* [aemim][$PF_6$] and [apbim][$BF_4$] were simulated in *NPT* ensemble at 1 atm and 298.15, 333.15, and 368.15 K. The calculated densities are presented in Table 1. Their densities ascend along with temperature decreasing. In the span of 70 K, the densities increase 0.048 g cm$^{-3}$ for [aemim][$PF_6$] and 0.05 g cm$^{-3}$ for [apbim][$BF_4$]. The simulated density for [aemim][$PF_6$] at 298.15 K is 1.54 g cm$^{-3}$, and it is in good agreement with the experimental value of 1.56 g cm$^{-3}$.[27] Comparing with [aemim][$PF_6$], the density of [apbim][$BF_4$] is lower, e.g., 1.203 g cm$^{-3}$ at 298.15 K. The lower density may be ascribed to the longer alkyl side chains of [apbim][$BF_4$] than [aemim][$PF_6$] which reduce the packing efficiency of the fluid.[14] When comparing with 1,3-dibutylimidazolium tetrafluoroborate ([bbim][$BF_4$], it has similar side-chain characteristic to [apbim][$BF_4$]), the density of [apbim][$BF_4$] is higher than that of [bbim][$BF_4$], e.g., 1.203 g cm$^{-3}$ for [apbim][$BF_4$] at 298.15 K while 1.15 g cm$^{-3}$ for [bbim][$BF_4$] at 301.15 K.[80] The higher density of [apbim][$BF_4$] partially results from the more compact ILs structure caused by amino-associated interaction, as will be illustrated.

*Energy analysis.* The calculated intermolecular energies in liquid phase ($U^{int}$, i.e., the sum of intermolecular van der Waals and Lennard-Jones energies), vaporization heat ($\Delta H^{vap}$), molar volume ($V_m$), and cohesive energy density ($c$), are presented in Table 1, see to Ref. 36 for the detailed description of calculating these energy terms.

Comparing with [bmim][$BF_4$] and [bmim][$PF_6$], amino-functionalized [aemim][$PF_6$] and [apbim][$BF_4$] give more negative $U^{int}$, e.g., −523.1 and −540.4 kJ mol$^{-1}$ for [aemim][$PF_6$] and [apbim][$BF_4$] at 298.15 K, respectively, while −493.8 and −506.8 kJ mol$^{-1}$ for [bmim][$PF_6$] and [bmim][$BF_4$],[36] respectively, which indicates the stronger ion interaction in [aemim][$PF_6$] and [apbim][$BF_4$]. In addition, the high vaporization heats and cohesive energy densities for [aemim][$PF_6$] and [apbim][$BF_4$] are consistent with the nature of negligible vapor pressure.

*Volume expansivity.* The volume expansivity indicates the extent to which the volume of a fluid changes with temperature at constant pressure, and is defined as

$$\alpha_p = \frac{1}{V}\left(\frac{\partial V}{\partial T}\right)_p \quad (1)$$

The calculated molar volumes as a function of temperature at 1 atm are shown in Figure 1, and their values are included in Table 1. Figure 1 shows that the change of molar volume

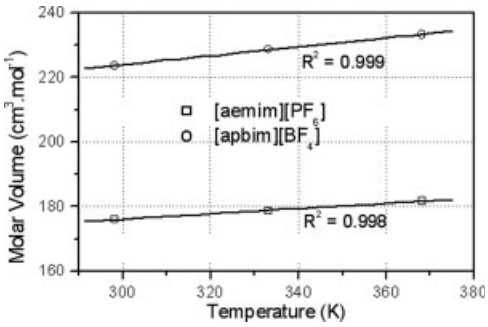


**Figure 1. Calculated molar volumes of [aemim][$PF_6$] and [apbim][$BF_4$] at 1 atm.**

Lines are linear fits to the data.

**Table 2. Characteristic Parameters for the RDFs Between P-Atom on $[PF_6]^-$ and Heavy Atoms on $[aemim]^+$, Along with the First Shell Integral Number *I(r)***

| | Characteristic Parameters (Å) | | | | | | |
|---|---|---|---|---|---|---|---|
| Site–Site | max$_1$* | min$_1$† | max$_2$ | min$_2$ | max$_3$ | min$_3$ | $I(r)$ |
| P—C2 | 3.95 | 5.05 | 6.25 | 7.75 | 10.45 | 14.25 | 1.98 |
| P—C4 | 4.25 | 5.05 | 5.45 | 7.15 | 11.45 | 14.85 | 2.12 |
| P—C5 | 4.35 | 5.05 | 5.45 | 6.95 | 11.25 | 14.85 | 2.01 |
| P—C9 | 4.55 | 7.05 | 10.75 | | | | 5.51 |
| P—C12 | 4.35 | 6.45 | 9.45 | | | | 4.39 |
| P—C16 | 4.55 | 6.85 | 9.55 | | | | 5.04 |
| P—N19 | 4.05 | 4.85 | 5.55 | 7.15 | 9.15 | | 1.86 |

*Location of the maximum of $g(r)$.
†Location of the minimum of $g(r)$.

with temperature is very linear. The calculated $\alpha_P$ of [aemim][$PF_6$] and [apbim][$BF_4$] are 4.59 × $10^{-4}$ $K^{-1}$ and 6.06 × $10^{-4}$ $K^{-1}$, respectively, which are comparable with the $\alpha_P$ of [bmim][$PF_6$] at 0.98 bar, 5.49 × $10^{-4}$ $K^{-1}$.[32]

*Liquid structure*. Site–site radial distribution functions (RDFs), $g(r)$, and site–site number integrals, $I(r)$, are used to characterize the liquid microstructure of [aemim][$PF_6$] and [apbim][$BF_4$], based on the results in *NPT* ensemble of 298.15 K and 1 atm. Here, two class of site–site RDFs were computed. One is between P-/B-atoms on anions and heavy atoms on cations, which reflects the organization of anions around cations. The other one is between F-atoms on anions and H-atoms on cations, which indicates the hydrogen bonding interaction between anions and cations.

The RDFs between P-atom on $[PF_6]^-$ and heavy atoms on $[aemim]^+$ are shown in Figure 2 and some selected characteristic parameters are presented in Table 2. As shown in Figure 2, four strong peaks of P—C2, P—N19, P—C4, and P—C5 indicate the strong organization of $[PF_6]^-$ around C2-site, C4-site, C5-site, and —$NH_2$. The first peak of P—C2 appears at 3.95 Å with an $I(r)$ of 1.98 at the first shell, which is similar to that in [bmim][$PF_6$] where the peak is observed at 4 Å with an $I(r)$ of 2.0[14]; the RDFs for P—C4 and P—C5 are almost identical, and their characteristics are comparable to that in [bmim][$PF_6$].[14,32] So, the amino addition does not has remarkable effects on the organization of $[PF_6]^-$ around C2-/C4-/C5-sites, instead, the —$NH_2$ participates in the cation–anion interaction as a new strong site. At first of sight, P—C9, P—C12, and P—C16 also give strong peaks, but they are pushed to further positions; as a matter of fact, C9-site, C12-site, and C16-site are only sharing the $[PF_6]^-$ which organize around C2-site, C4-site, C5-site, and —$NH_2$. Table 2 indicates that at the first shell there are 1.98, 2.12, 2.01, and 1.86 anions around C2-site, C4-site, C5-site, and —$NH_2$, respectively, and thus there are totally 7–8 anions around the cation at the first shell.

The RDFs between F-atoms on $[PF_6]^-$ and H-atoms on $[aemim]^+$ are shown in Figure 3. Because of the fact that the H-atoms on the same heavy atom give almost completely identical RDFs, only one H-atom on each heavy atom is selected to present the RDFs. As shown in Figure 3, there are four strong peaks, i.e., F—H6, F—H7, F—H8, and F—H20; further, their peak positions are at 2.25, 2.55, 2.55, and 2.15 Å, respectively, and they are all less than the the van der Waals H···F distance of 2.7 Å.[81] Thus, there exist strong hydrogen bonding interaction between H6, H7, H8, H20/H21 and the F-atoms of $[PF_6]^-$, which is consistent with the strong organization of $[PF_6]^-$ around C2-site, C7-site, C8-

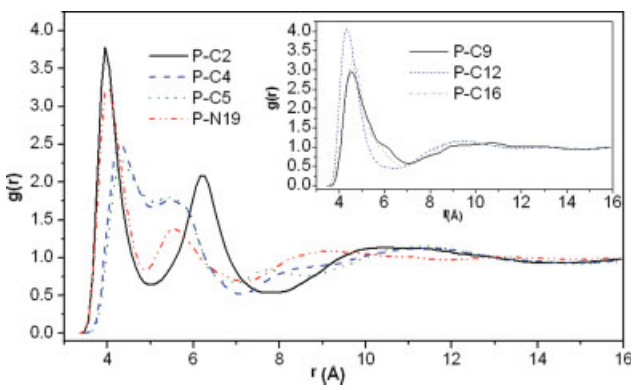


**Figure 2. RDFs presentation between P-atom on $[PF_6]^-$ and heavy atoms on $[aemim]^+$ (see Figure S1a for atom numbering).**

[Color figure can be viewed in the online issue, which is available at www.interscience.wiley.com.]

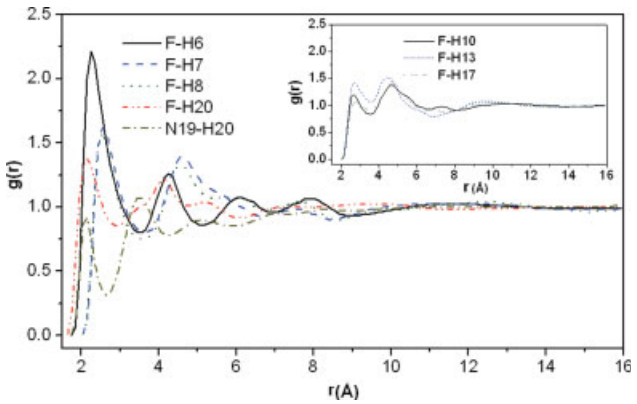


**Figure 3. RDFs presentation between F-atoms on $[PF_6]^-$ and H-atoms on $[aemim]^+$ (see Figure S1a for atom numbering).**

[Color figure can be viewed in the online issue, which is available at www.interscience.wiley.com.]

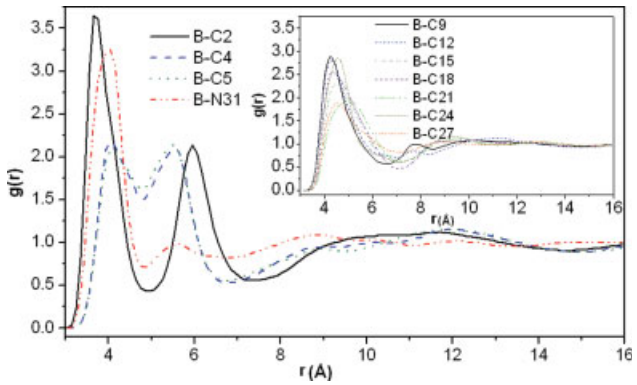


**Figure 4. RDFs presentation between B-atom on $[BF_4]^-$ and heavy atoms on $[apbim]^+$ (see Figure S1b for atom numbering).**

[Color figure can be viewed in the online issue, which is available at www.interscience.wiley.com.]

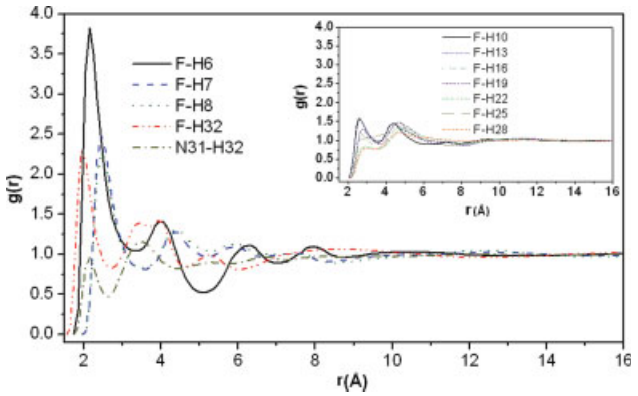


**Figure 5. RDFs presentation between F-atoms on $[BF_4]^-$ and H-atoms on $[apbim]^+$ (see Figure S1b for atom numbering).**

[Color figure can be viewed in the online issue, which is available at www.interscience.wiley.com.]

site, and $-NH_2$ discussed earlier. There are much weaker hydrogen bonding interaction between the F-atoms and the remained H-atoms on the side-chains. An interesting finding is that F-H17 presents a peak while the counterpart F—HC in [bmim][$PF_6$] (see Figure 5 in Ref. 36) does not, which implies that H17 is sharing the anions that interact with $-NH_2$. In addition, the RDFs for N19—H20 shows that there does not exist remarkable hydrogen bonding interaction between the $-NH_2$ on different cations.

The RDFs between B-atom on $[BF_4]^-$ and heavy atoms on $[apbim]^+$ are shown in Figure 4, and some selected characteristic parameters are presented in Table 3. The RDFs between F-atoms on $[BF_4]^-$ and H-atoms on $[apbim]^+$ are shown in Figure 5. As shown in Figure 4 and 5, similar to [aemim][$PF_6$], in [apbim][$BF_4$] the $-NH_2$ is a new strong cation–anion interaction site. $[BF_4]^-$ organizes around C2-site, C4-site, C5-site, and $-NH_2$, and forms the hydrogen bonds with the H-atoms on these sites. Table 3 shows that there are totally 5–6 $[BF_4]^-$ around $[apbim]^+$. In Figure 4, the first and second peaks of B—C4 and B—C5 are very close, only 1.5 and 1.4 Å, respectively, and the close second peaks are expected to be partially intervened by the $[BF_4]^-$ around C2-site.[14] Because of the almost completely symmetric side chains in $[apbim]^+$, the RDFs between B-atom and the counterpart C-atoms on two side chains were expectedly similar; however, comparing with B—C15 (4.45 Å)/B—C21 (5.05 Å)/B—C27 (4.55 Å), B—C18, and B—C24 give higher peaks at closer 4.35 and 4.55 Å, respectively, which are expected to result from the effects of $[BF_4]^-$ around terminal $-NH_2$. In Figure 5, the weak F—H25/H26 are out of our expectation, because H25/H26 are just next to the terminal $-NH_2$ and were expected to interact with the $[BF_4]^-$ around $-NH_2$; otherwise, this possibly implies that the orientation for $[BF_4]^-$ to approach $-NH_2$ is from C24—N31 axis. The RDFs for N31—H32 indicates in [apbim][$BF_4$] the $-NH_2$ on different cations do not remarkably interact.

**Table 3. Characteristic Parameters for the RDFs Between B-atom of $[BF_4]^-$ and Heavy Atoms on $[apbim]^+$, Along with the First Shell Integral Number $I(r)$**

| | Characteristic Parameters (Å) | | | | | | |
|---|---|---|---|---|---|---|---|
| Site–Site | $max_1$* | $min_1$† | $max_2$ | $min_2$ | $max_3$ | $min_3$ | $I(r)$ |
| B—C2 | 3.65 | 4.95 | 5.95 | 7.35 | 11.65 | 14.65 | 1.59 |
| B—C4 | 4.05 | 4.75 | 5.55 | 6.75 | 11.95 | 14.95 | 1.29 |
| B—C5 | 4.05 | 4.75 | 5.45 | 6.75 | 11.95 | 15.05 | 1.27 |
| B—C9 | 4.25 | 6.55 | | | | | 3.50 |
| B—C12 | 4.25 | 7.05 | | | | | 4.37 |
| B—C15 | 4.45 | 7.25 | 8.85 | | | | 4.41 |
| B—C18 | 4.35 | 7.05 | | | | | 4.39 |
| B—C21 | 5.05 | 7.15 | 9.75 | | | | 4.39 |
| B—C24 | 4.55 | 7.15 | 9.25 | | | | 4.33 |
| B—C27 | 4.55 | 7.15 | 8.95 | | | | 4.23 |
| B—N31 | 4.05 | 4.85 | | | | | 1.68 |

*Location of the maximum of $g(r)$.
†Location of the minimum of $g(r)$.

The center-of-mass RDFs for cation–cation, anion–anion, and anion–cation of [aemim][$PF_6$] and [apbim][$BF_4$] are shown in Figure 6, and some selected characteristic parameters are presented in Table 4. In [aemim][$PF_6$], the RDFs for cation–anion indicates that there are three solvation shells in half a simulation box; the $I(r)$ of 7.57 at the first shell is consistent with the foregoing RDFs results between P-atom on $[PF_6]^-$ and heavy atoms on $[aemim]^+$. In [apbim][$BF_4$], the first peak of cation–anion RDFs is slit into two subpeaks with comparable height and close distance of 1.7 Å. Combining Figure 4 and Table 3, the first subshell is expected to be associated with C2-site, the second with $-NH_2$, and C4-/C5-sites are probably involved in both of the subshells. The $I(r)$ of 5.19 at the first shell is also consistent with the foregoing RDFs results between B-atom of $[BF_4]^-$ and heavy atoms on $[apbim]^+$.

The above MD simulation results show that, in [aemim][$PF_6$] and [apbim][$BF_4$], besides the well-known C2-, C4-, and C5-sites, terminal $-NH_2$ participates in the cation–anion interaction as a new strong site. The anions interacting with $-NH_2$ may simultaneously interact with other cations through C2-/C4-/C5-sites or $-NH_2$, thus, a compact liquid structure in such amino-functionalized imidazolium ILs is formed with the participation of $-NH_2$. In such liquids, the ion fragments are relatively stably "fixed" and the ion motion becomes more difficult. To more quantitatively

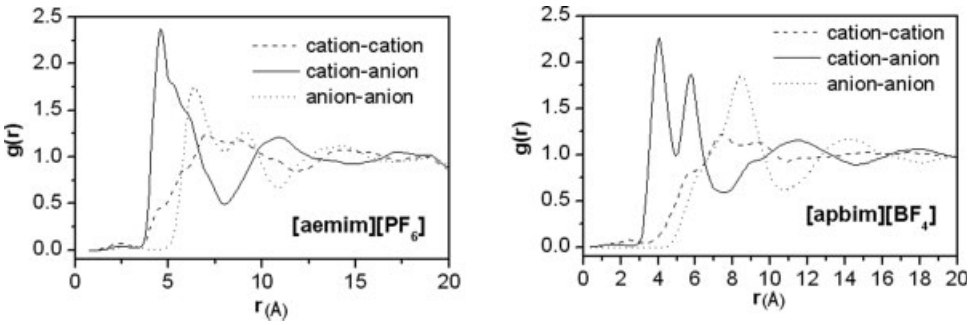


**Figure 6. Center-of-mass RDFs presentation for ion–ion of [aemim][$PF_6$] and [apbim][$BF_4$].**

understand such amino-associated interaction, a statistic on the number of anions that undergo hydrogen bonding interaction with $-NH_2$ was performed, and the results are presented in Table 5. As presented in Table 5, there are around 83.6% and 81.7% anions being involved in the interaction with $-NH_2$ for [aemim][$PF_6$] and [apbim][$BF_4$], respectively. Further, the numbers of the anions that simultaneously interact with two $-NH_2$ or more are 51% and 44.9% for [aemim][$PF_6$] and [apbim][$BF_4$], respectively, which indicates a local network-characteristic liquid structure. So, a great portion of the cation–anion interaction are concerned with $-NH_2$. As a comparison, although there are similar chemical environments for the terminal $-CH_3$ and $-NH_2$ on $[apbim]^+$, there are only 34.1% anions interacting with the terminal $-CH_3$ and only 6.0% simultaneously with two $-CH_3$ or more. Thus, the participation of $-NH_2$ in the cation–anon interaction is believed to be responsible for their higher viscosities.

*Self-diffusion coefficient.* The self-diffusion coefficient, $D$, is calculated by the Einstein relation.[72]

$$D = \frac{1}{6} \lim_{t\to\infty} \frac{d}{dt} \langle \Delta r(t)^2 \rangle \tag{2}$$

where $\Delta r(t)^2$ is the mean square displacement (MSD) of the center-of-mass of a molecule, and "$\langle\rangle$" represents ensemble average. The MSDs of the cations and anions for [aemim][$PF_6$] and [apbim][$BF_4$] at 298.15 K and 1 atm are shown in Figure 7. Both of the MSDs for [aemim][$PF_6$] and [apbim][$BF_4$] are roughly linear with the time from 1000 to 2000 ps, and their self-diffusion coefficients for the cations and anions were obtained by fitting the slope of this linear region. The calculated self-diffusion coefficients are presented in Table 1. The self-diffusion coefficients of the cations are higher than that of the anions, which is also found in conventional imidazolium hexafluorophosphate and tetrafluoroborate ILs.[32,33,36,45,65,82] Table 1 shows that the self-diffusion coefficients are sensitive to temperature, which is also consistent with the experimental observation.[65] The self-diffusion coefficients of [aemim][$PF_6$] and [apbim][$BF_4$] are on the order of $10^{-13}$ $m^2$ $s^{-1}$ at 298.15 K, which is roughly 2 order of magnitude lower than that of conventional imidazolium hexafluorophosphate and tetrafluoroborate ILs,[32,33,36,45] and this is consistent with the higher viscosities of the formers.

*Ab Initio Calculations of Ion Pair.* Ab initio calculations of isolated ion pair of imidazolium ILs showed that the cation–anion interaction characteristic in ion pair is in agreement with that in bulk liquid, [49–54,56–58] such as the C2-site, C4-site, and C5-site on imidazolium ring that were found to be the main cation–anion interaction sites both from ab initio calculations of ion pair and MD simulations of bulk liquid. Ab initio calculations of ion pair can be employed to investigate the local interaction on individual ions within ILs, such as cation–anion interaction site, hydrogen bond, and cation–anion interaction energy, and so on.

*[aemim][$PF_6$].* The starting structures were constructed through placing $[PF_6]^-$ in various positions around $[aemim]^+$. Following the previous calculated results for imidazolium ILs ion pair,[49–54,56–58] the regions on $[aemim]^+$ to be considered for potential interaction with $[PF_6]^-$ mainly include (a) both the side chains (potential van der Waals and hydrogen bonding interaction), (b) the top and bottom of imidazolium ring plane (possible interaction with $\pi$ electrons), and (c) the three ring H-sites on C2/C4/C5 (coupled hydrogen bonding and electrostatic interaction), see Figure S1a for a visual understanding. The final stable configurations obtained at MP2/6-31G* level are shown in Figure 8. The configurations obtained at B3LYP/6-31G* level (see Figure S3) are comparable with that at MP2/6-31G* level. Although there are

**Table 4. Characteristic Parameters for the Cation–Anion Center-of-Mass RDFs of [aemim][$PF_6$] and [apbim][$BF_4$], Along with the First Shell Integral Number $I(r)$**

| | Characteristic Parameters (Å) | | | | | | | |
|---|---|---|---|---|---|---|---|---|
| Cation-Anion | $max_1$* | $min_1$† | $max_2$ | $min_2$ | $max_3$ | $min_3$ | $max_4$ | $I(r)$ |
| $[aemim]^+$-$[PF_6]^-$ | 4.55 | 7.95 | 10.85 | 14.85 | 17.25 | | | 7.57 |
| $[apbim]^+$-$[BF_4]^-$ | 4.05 | 4.95 | 5.75 | 7.55 | 11.45 | 14.65 | 17.95 | 5.19‡ |

*Location of the maximum of $g(r)$.
†Location of the minimum of $g(r)$.
‡The $I(r)$ is up to $min_2$.

**Table 5. Statistic on the Number of Anions Undergoing Hydrogen Bonding Interaction with $-NH_2$, along with the Terminal $-CH_3$ in [apbim][$BF_4$]**

| | | | | | | | |
|---|---|---|---|---|---|---|---|
| [aemim][$PF_6$] | | | | | | | |
| $-NH_2$ coordination no.* | 0 | 1 | 2 | 3 | 4 | 5 | 6 |
| $[PF_6]^-$ no. | 31.4 ± 1.8 | 62.5 ± 2.9 | 57.6 ± 2.6 | 29.0 ± 1.4 | 10.0 ± 1.5 | 1.4 ± 0.4 | 0.1 ± 0.1 |
| $[PF_6]^-$ no./ total $[PF_6]^-$ no. % | 16.4 ± 0.9 | 32.6 ± 1.5 | 30.0 ± 1.3 | 15.1 ± 0.7 | 5.2 ± 0.8 | 0.7 ± 0.2 | 0.1 ± 0.0 |
| [apbim][$BF_4$] | | | | | | | |
| $-NH_2$ coordination no.* | 0 | 1 | 2 | 3 | 4 | 5 | 6 |
| $[BF_4]^-$ no. | 35.2 ± 3.6 | 70.6 ± 4.2 | 57.2 ± 3.9 | 23.5 ± 2.7 | 4.7 ± 0.9 | 0.7 ± 0.6 | 0.0 ± 0.1 |
| $[BF_4]^-$ no./ total $[BF_4]^-$ no. % | 18.3 ± 1.9 | 36.8 ± 2.2 | 29.8 ± 2.0 | 12.3 ± 1.4 | 2.5 ± 0.5 | 0.4 ± 0.3 | 0.0 |
| [apbim][$BF_4$] | | | | | | | |
| $-CH_3$ coordination no.† | 0 | 1 | 2 | 3 | 4 | 5 | 6 |
| $[BF_4]^-$ no. | 126.6 ± 1.5 | 54.0 ± 1.5 | 10.2 ± 0.5 | 1.1 ± 0.1 | 0.1 ± 0.0 | 0.0 | 0.0 |
| $[BF_4]^-$ no./ total $[BF_4]^-$ no. % | 65.9 ± 0.8 | 28.1 ± 0.8 | 5.3 ± 0.3 | 0.6 ± 0.0 | 0.0 ± 0.0 | 0.0 | 0.0 |

*The number of $-NH_2$ simultaneously interacting with an anion.
†The number of $-CH_3$ simultaneously interacting with an anion.

some little deviations for some specific hydrogen bonds, the main cation–anion interaction characteristics are identical. So, only the ion pairs obtained at MP2/6-31G* level are discussed.

As shown in Figure 8, configuration 8a is the most stable. The energies of configurations 8b, 8c, and 8d are 11.4, 36.4, and 57.8 kJ $mol^{-1}$ higher than that of 8a, respectively. In the most stable 8a, the terminal $—NH_2$ is involved in hydrogen bonding interaction with $[PF_6]^-$. The hydrogen bonding strength is comparable with that between C2—H and $[PF_6]^-$, as indicated by the hydrogen bonding parameters for N—H···F (NH···F, 2.15 Å, < (N—H···F), 137.6°) and C2—H···F (C2H···F, 2.09/2.10 Å, < (N—H···F), 138.7/130.2°), while stronger than other hydrogen bonds on alkyl side chains. Such a hydrogen bond characteristic is different from that in conventional imidazolium ILs, in the latter the hydrogen atoms on further than the ethyl C of side chain are not involved in hydrogen bonds for an ion pair.[49–54,56,57] When the amino-associated hydrogen bond is excluded, e.g., 8b, the ion pair steps into higher-energy configurations. Further, when the C2—H is also excluded, e.g., 8c and 8d, the energies of the ion pairs are significantly increased. Thus, besides C2—H, the terminal $—NH_2$ is another new interaction site which is consistent with the above MD simulation results, and the involution of $—NH_2$ enhances the cation–anion interaction in [aemim][$PF_6$].

The cation–anion interaction energy of ILs, $U^{\text{ion pair}}$, is defined as the difference between the energy of the ion pair and the sum of the energies of the purely cationic and anionic species, which indicates the strength of cation–anion interaction. The values of $U^{\text{ion pair}}$ for [aemim][$PF_6$], along with [bmim][$PF_6$] and [bmim][$BF_4$], are presented in Table 6. As indicated in Table 6, [aemim][$PF_6$] has a more negative $U^{\text{ion pair}}$, i.e., stronger cation–anion interaction.

*[apbim][$BF_4$].* The construction of starting structures for [apbim][$BF_4$] is similar to that for [aemim][$PF_6$]. The final stable configurations at MP2/6-31G* level are shown in Figure 9 and that at B3LYP/6-31G* level are shown in Figure S4.

As shown in Figure 9, configuration 9a is the most stable, of which the energy is 19.3, 45.3, and 45.9 kJ $mol^{-1}$ lower than that of configurations 9b, 9c, and 9d, respectively. Similar to the most stable configuration 8a for [aemim][$PF_6$], in configuration 9a the terminal $—NH_2$ is also involved in the hydrogen bonding interaction with the anion, again, the hydrogen bonding strength between $—NH_2$ and $[BF_4]^-$ is comparable with that between C2—H and $[BF_4]^-$, as indicated by the hydrogen bonding parameters for N—H···F (NH···F, 2.00 Å, < (N—H···F), 154.4°) and C2—H···F (C2H···F, 2.05, < (N—H···F), 144.9°), while stronger than other hydrogen bonds on alkyl side chains. When the $—NH_2$ is excluded from hydrogen bond, a 19.3 kJ $mol^{-1}$ energy is increased for configuration 9b. When both $—NH_2$ and C2 are excluded, i.e., in the case of configurations 9c and 9d, the energies are significantly increased. The relative energies of configurations 9c and 9d are comparable while there is a large energy difference between configurations 8c and 8d of [aemim][$PF_6$], which is ascribed to the more symmetrical alkyl side chains in [apbim][$BF_4$]. The above results show

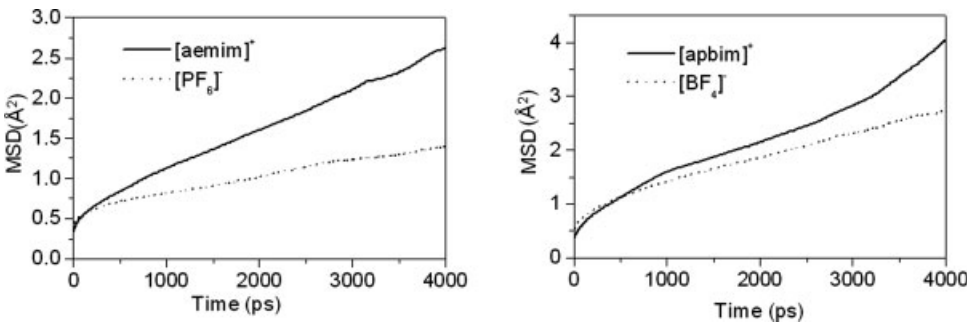


**Figure 7. Center of mass mean square displacements of [aemim][$PF_6$] and [apbim][$BF_4$] at 298.15 K and 1 atm.**

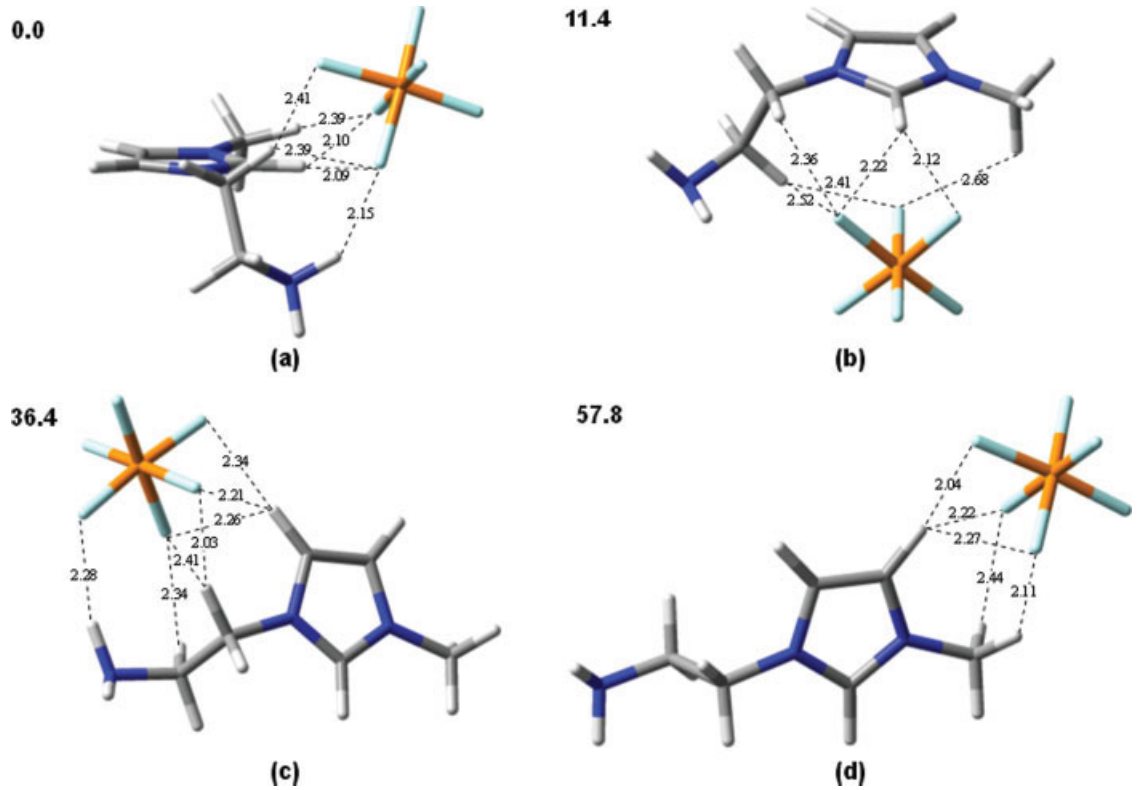


**Figure 8. The stable configurations for [aemim][$PF_6$] ion pair, calculated at MP2/6-31G* level; hydrogen bonds are indicated by dot line and distances are in Å; the relative energy values are labeled on the top-left corner of each configuration, in kJ $mol^{-1}$.**

[Color figure can be viewed in the online issue, which is available at www.interscience.wiley.com.]

that in [apbim][$BF_4$], the amino-associated hydrogen bond enhances the cation–anion interaction. The values of $U^{\text{ion pair}}$ in Table 6 also show a stronger cation–anion interaction in [apbim][$BF_4$] than that in those without —$NH_2$.

*Ion tripolymer*. As indicated in the earlier MD simulations, in the bulk liquids the cations are generally surrounded by several anions. Therefore, another anion is added into the above ion pairs to construct ion tripolymer unit. The stable tripolymers for [aemim][$PF_6$] and [apbim][$BF_4$] are shown in Figure 10. As shown in Figure 10, the addition of the second anions does not remarkably change the cation–anoin interaction characteristics of the original ion pairs, and only has some effects on some specific hydrogen bonding parameters, e.g., the F—NH bond in [aemim][$PF_6$] is slightly lengthened from 2.15 to 2.21 Å and the F—NH bond in [apbim][$BF_4$] is lengthened from 2.00 to 2.03 Å. In these tripolymers, C2-site, C4-site, and —$NH_2$ are simultaneously involved into the interaction with anions, and the local liquid structure is closer to these tripolymer units.

**Table 6. Cation–Anion Interaction Energies (in kJ $mol^{-1}$) for Imidazolium ILs**

| | Interaction Energy | |
|---|---|---|
| ILs | B3LYP/6-31G* | MP2/6-31G* |
| [aemim][$PF_6$] | −393.0 | −402.3 |
| [bmim][$PF_6$] | −370.2 | −376.6 |
| [apbim][$BF_4$] | −425.5 | −435.0 |
| [bmim][$BF_4$] | −403.2 | −406.0 |

*Rotation of side-chain with —$NH_2$*. To investigate the influences of amino-associated hydrogen bonds on the flexibility of the related side chain, the relaxed energy scans for the rotation of the side chain with —$NH_2$ are performed with the existence of one anion, two anions, and no anions. The results are shown in Figure 11. Comparing with [aemim][$PF_6$], the influences of the addition of anions on the rotation of —$NH_2$ side-chain is somewhat more complicated. As indicated in Figure 11, the hydrogen bonds between —$NH_2$ and anions increase the rotational energy barriers of side chain and reduce the flexibility. Following the previous understanding that the flexibility of side chain will impose important effects on ILs viscosity,[59–61] the interaction between —$NH_2$ and anions is partially responsible for their high viscosities.

## Conclusions

To understand the functional ILs from a microscopic point of view and promote their applications in industry, in this work, the microstructure, interionic interaction, and properties of two selected amino-functionalized imidazolium ILs, [aemim][$PF_6$] and [apbim][$BF_4$], are studied by using ab initio calculations and MD simulations, specifically, including

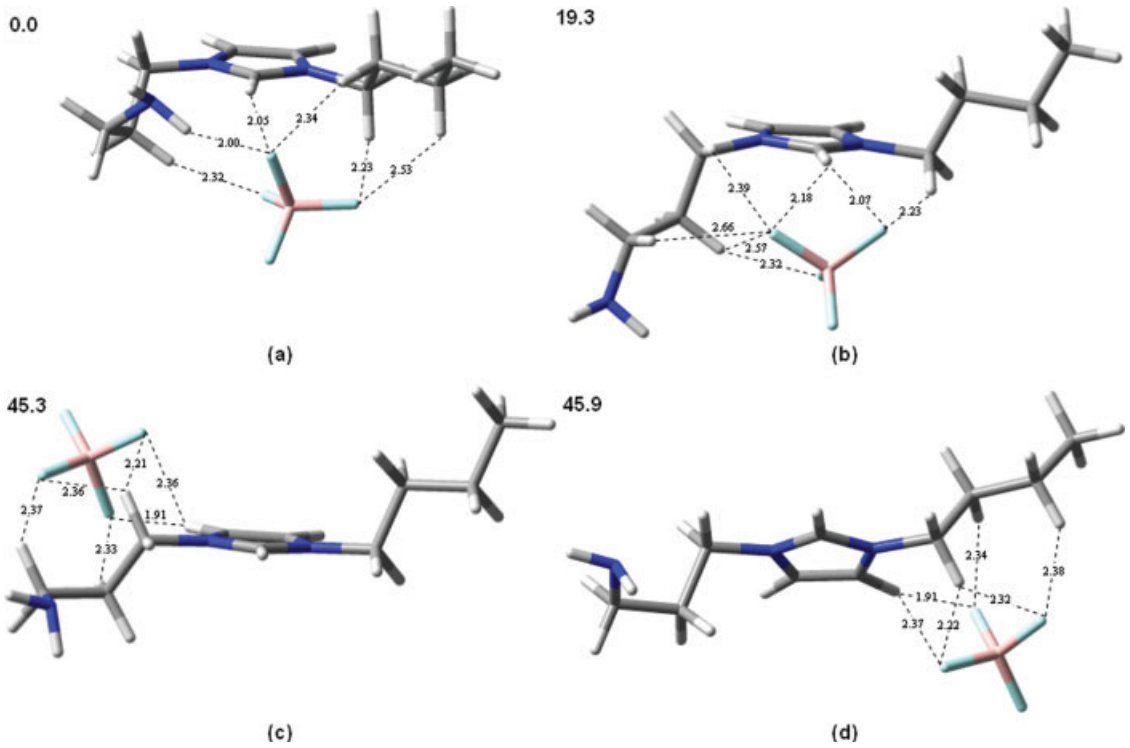


**Figure 9. The stable configurations for [apbim][$BF_4$] ion pair, calculated at MP2/6-31G* level; hydrogen bonds are indicated by dot line and distances are in Å; the relative energy values are labeled on the top-left corner of each configuration, in kJ $mol^{-1}$.**

[Color figure can be viewed in the online issue, which is available at www.interscience.wiley.com.]

the cation–anion interaction pattern, interaction energy, hydrogen bond, and the flexibility of side chain rotation in the isolated ion pairs; the density, energy composition, volume expansivity, ionic organization (site-site RDFs), hydrogen bond, and self-diffusion coefficient in the bulk liquids.

It is found that the amino addition does not remarkably affect the organization of anions around C2-site, C4-site, and C5-site on imidazolium ring, instead, —$NH_2$ participates in the cation–anion interaction as a new strong site. In their bulk liquids, the site–site radial distribution functions (RDFs) between P-/B-atoms on their anions and heavy atoms on their cations indicate that the anions strongly organize around —$NH_2$, further, the RDFs between F-atoms and H-atoms indicate that —$NH_2$ forms hydrogen bonds with the anions.

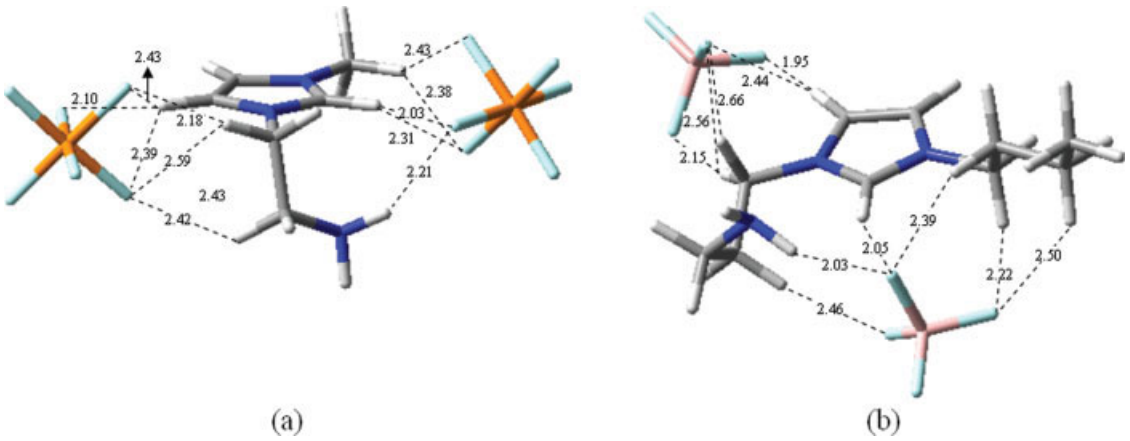


**Figure 10. The stable ion tripolymers for (a) [aemim][$PF_6$] and (b) [apbim][$BF_4$], calculated at B3LYP/6-31G* level.**

[Color figure can be viewed in the online issue, which is available at www.interscience.wiley.com.]

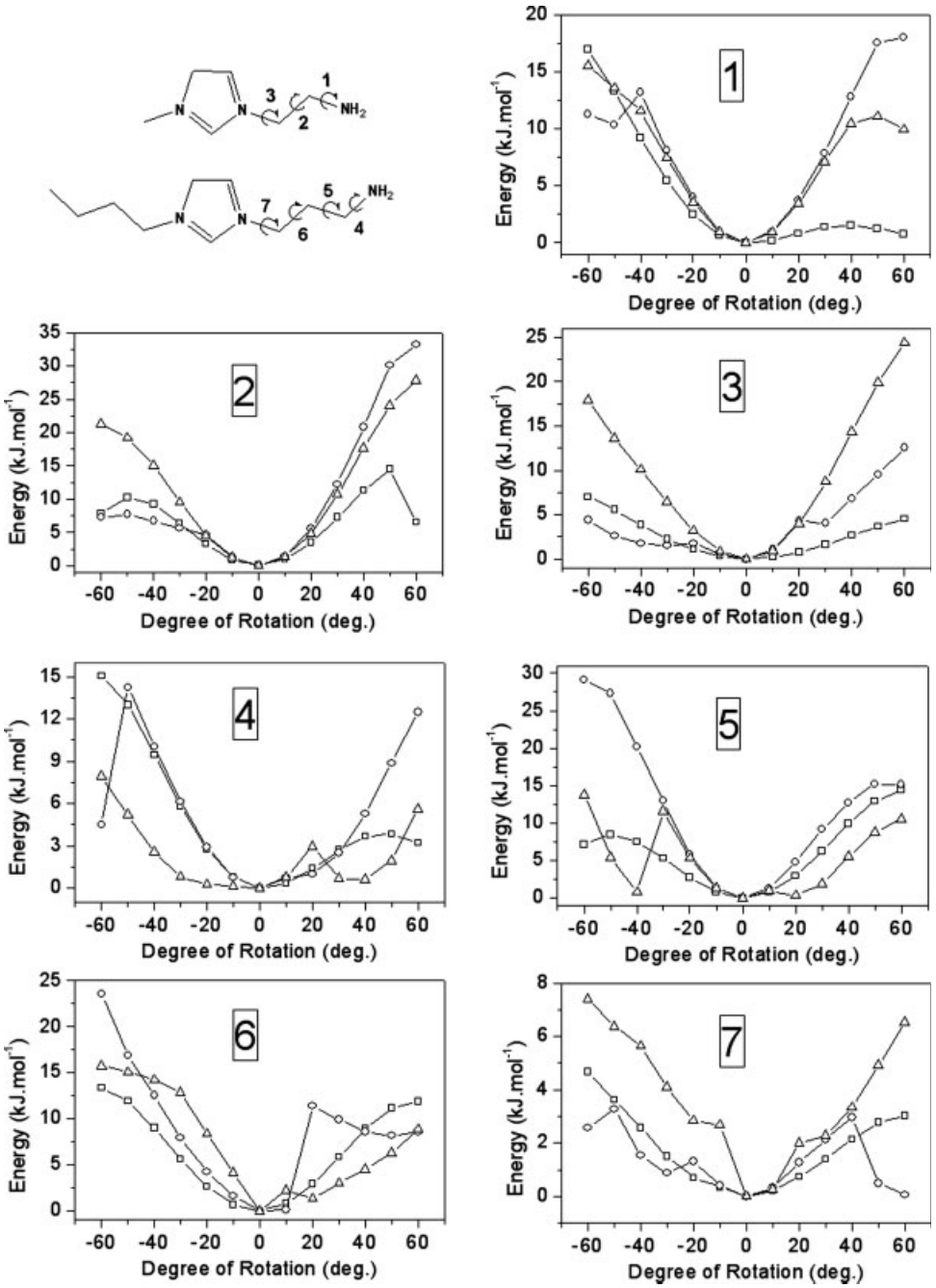


**Figure 11. The rotation of side chain with $-NH_2$ for [aemim][$PF_6$] and [apbim][$BF_4$] at B3LYP/6-31G* level, with the existence of one anion (circle, ○), two anions (triangle, △), and no anions (square, □).**

The abscissas and ordinate denote the rotational degrees and energies relative to the stable configurations.

Such a participation of $-NH_2$ in cation–anion interaction may result into a local network-characteristic and more compact liquid structure. The simulated ionic self-diffusion coefficients are on the order of $10^{-13}$ $m^2$ $s^{-1}$ at 298.15 K, roughly 2 order of magnitude lower than that of conventional imidazolium ILs, which is qualitatively consistent with their higher experimental viscosities. In their most stable ion pair configurations, terminal $-NH_2$ forms hydrogen bonds with anions, furthermore, the hydrogen bonding strength is comparable with that of C2—H on imidazolium ring and much stronger than that of other alkyl H-atoms. The amino-associated hydrogen bonds reduce the flexibility of alkyl side chains, and the cation–anion interaction energies are 20–30 kJ $mol^{-1}$ higher than that of some imidazolium ILs without $-NH_2$.

This work shows that side chains of imidazolium ring may play an important role in deciding ILs structure/property, and should be carefully tailored in ILs design.

## Acknowledgments

This work was financially supported by National Science Fund of China for Distinguished Young Scholar (20625618) and National Natural Science Foundation of China (20603040). The Super Computing Center of Chinese Academy of Sciences is also highly appreciated for generously providing the computer sources.

## Literature Cited

1. Welton T. Room-temperature ionic liquids. Solvents for synthesis and catalysis. *Chem Rev*. 1999;99:2071–2083.
2. Holbrey JD, Seddon KR. Ionic liquids. *Clean Prod Process*. 1999;1:223–236.
3. Brennecke JF, Maginn EJ. Ionic liquids: innovative fluids for chemical processing. *AIChE J*. 2001;47:2384–2389.
4. Dupont J, de Souza RF, Suarez PAZ. Ionic liquid (molten salt) phase organometallic catalysis. *Chem Rev*. 2002;102:3667–3692.
5. Rogers RD, Seddon KR, editors. *Ionic Liquids: Industrial Applications to Green Chemistry*. Washington, DC: Oxford University Press, 2002.
6. Rogers RD, Seddon KR, editors. *Ionic Liquids as Green Solvents: Progress and Prospects*. Washington, DC: Oxford University Press, 2002.
7. Rogers RD, Seddon KR. Ionic liquids—Solvents of the future? *Science*. 2003;302:792–793.
8. Marsh KN, Boxall JA, Lichtenthaler R. Room temperature ionic liquids and their mixtures—a review. *Fluid Phase Equilib*. 2004; 219:93–98.
9. Zhang SJ, Sun N, He XZ, Lu XM, Zhang XP. Physical properties of ionic liquids: database and evaluation. *J Phys Chem Ref Data*. 2006; 35:1475–1517.
10. Blanchard LA, Gu ZY, Brennecke JF. High-pressure phase behavior of ionic liquid/$CO_2$ systems. *J Phys Chem B*. 2001;105: 2437–2444.
11. Husson-Borg P, Majer V, Costa Gomes MF. Solubilities of oxygen and carbon dioxide in butyl methyl imidazolium tetrafluoroborate as a function of temperature and at pressures close to atmospheric pressure. *J Chem Eng Data*. 2003;48:480–485.
12. Kamps APS, Tuma D, Xia JZ, Maurer G. Solubility of $CO_2$ in the ionic liquid [bmim][$PF_6$]. *J Chem Eng Data*. 2003;48:746–749.
13. Shariati, A, Peters CJ. High-pressure phase behavior of systems with ionic liquids. III. The binary system carbon dioxide+1-hexyl-3-methylimidazolium hexafluorophosphate. *J Supercrit Fluids*. 2004; 30:139–144.
14. Cadena C, Anthony JL, Shah JK, Morrow TI, Brennecke JF, Maginn EJ. Why is $CO_2$ so soluble in imidazolium-based ionic liquids? *J Am Chem Soc*. 2004;126:5300–5308.
15. Baltus RE, Culbertson BH, Dai S, Luo HM, De Paoli DW. Low-pressure solubility of carbon dioxide in room-temperature ionic liquids measured with a quartz crystal microbalance. *J Phys Chem B*. 2004;108:721–727.
16. Aki SNVK, Mellein BR, Saurer EM, Brennecke JF. High-pressure phase behavior of carbon dioxide with imidazolium-based ionic liquids. *J Phys Chem B*. 2004;108:20355–20365.
17. Scovazzo P, Camper D, Kieft J, Poshusta J, Koval C, Noble, R. Regular solution theory and $CO_2$ gas solubility in room-temperature ionic liquids. *Ind Eng Chem Res*. 2004;43:6855–6860.
18. Shariati A, Gutkowski K, Peters CJ. Comparison of the phase behavior of some selected binary systems with ionic liquids. *AIChE J*. 2005;51:1532–1540.
19. Shiflett MB, Yokozeki A. Solubilities and diffusivities of carbon dioxide in ionic liquids: [bmim][$PF_6$] and [bmim][$BF_4$]. *Ind Eng Chem Res*. 2005;44:4453–4464.
20. Huang XH, Margulis CJ, Li YH, Berne BJ. Why is the partial molar volume of $CO_2$ so small when dissolved in a room temperature ionic liquid? Structure and dynamics of $CO_2$ dissolved in [Bmim] [$PF_6$]. *J Am Chem Soc*. 2005;127:17842–17851.
21. Jacquemin J, Gomes MFC, Husson P, Majer V. Solubility of carbon dioxide, ethane, methane, oxygen, nitrogen, hydrogen, argon, and carbon monoxide in 1-butyl-3-methylimidazolium tetrafluoroborate between temperatures 283 K and 343 K and at pressures close to atmospheric. *J Chem Thermodyn*. 2006;38:490–502.
22. Kumelan J, Kamps IPS, Tuma D, Maurer G. Solubility of $CO_2$ in the ionic liquid [hmim][$Tf_2N$]. *J Chem Thermodyn*. 2006;38:1396–1401.
23. Gutkowski KI, Shariati A, Peters CJ. High-pressure phase behavior of the binary ionic liquid system 1-octyl-3-methylimidazolium tetrafluoroborate plus carbon dioxide. *J Supercrit Fluids*. 2006;39:187–191.
24. Kumelan J, Kamps APS, Tuma D, Maurer G. Solubility of $CO_2$ in the ionic liquids [bmim][$CH_3SO_4$] and [bmim][$PF_6$]. *J Chem Eng Data*. 2006;51:1802–1807.
25. Jacquemin J, Husson P, Majer V, Gomes MFC. Low-pressure solubilities and thermodynamics of solvation of eight gases in 1-butyl-3-methylimidazolium hexafluorophosphate. *Fluid Phase Equilib*. 2006; 240:87–95.
26. Shiflett MB, Yokozeki A. Solubility of $CO_2$ in room temperature ionic liquid [hmim][$Tf_2N$]. *J Phys Chem B*. 2007;111:2070–2074.
27. Song G, Cai Y, Peng Y. Amino-functionalized ionic liquid as a nucleophilic scavenger in solution phase combinatorial synthesis. *J Comb Chem*. 2005;7:561–566.
28. Bates ED, Mayton RD, Ntai I, Davis JH Jr. $CO_2$ capture by a task-specific ionic liquid. *J Am Chem Soc*. 2002;124:926–927.
29. Cai Y, Peng Y, Song G. Amino-functionalized ionic liquid as an efficient and recyclable catalyst for Knoevenagel reactions in water. *Catal Lett*. 2006;109:61–64.
30. Hanke CG, Price SL, Lynden-Bell RM. Intermolecular potentials for simulations of liquid imidazolium salts. *Mol Phys*. 2001;99:801–809.
31. Margulis CJ, Stern HA, Berne BJ. Computer simulation of a "green chemistry" room-temperature ionic solvent. *J Phys Chem B*. 2002; 106:12017–12021.
32. Morrow TI, Maginn EJ. Molecular dynamics study of the ionic liquid 1-*n*-butyl-3-methylimidazolium hexafluorophosphate. *J Phys Chem B*. 2002;106:12807–12813.
33. de Andrade J, Böes ES, Stassen H. Computational study of room temperature molten salts composed by 1-alkyl-3-methylimidazolium cations—Force-field proposal and validation. *J Phys Chem B*. 2002; 106:13344–13351.
34. Chaumont A, Engler E, Wipff G. Uranyl and strontium salt solvation in room-temperature ionic liquids. A molecular dynamics investigation. *Inorg Chem*. 2003;42:5348–5356.
35. del Popolo MG, Voth GA. On the structure and dynamics of ionic liquids. *J Phys Chem B*. 2004;108:1744–1752.
36. Liu ZP, Huang SP, Wang WC. A refined force field for molecular simulation of imidazolium-based ionic liquids. *J Phys Chem B*. 2004;108:12978–12989.
37. Lopes JNC, Pádua AAH. Molecular force field for ionic liquids composed of triflate or bistriflylimide anions. *J Phys Chem B*. 2004;108:16893–16898.
38. Deschamps J, Costa Gomes MF, Pádua AAH. Molecular simulation study of interactions of carbon dioxide and water with ionic liquids. *ChemPhysChem*. 2004;5:1049–1052.
39. Urahata SM, Ribeiro MCC. Structure of ionic liquids of 1-alkyl-3-methylimidazolium cations: a systematic computer simulation study. *J Chem Phys* 2004;120:1855–1863.
40. Alavi S, Thompson DL. Molecular dynamics studies of melting and some liquid-state properties of 1-ethyl-3-methylimidazolium hexafluorophosphate [emim][$PF_6$]. *J Chem Phys*. 2005;122:54704.
41. Liu XP, Liu ZP, Huang SP, Wang WC. Molecular dynamics simulation of room-temperature ionic liquid mixture of [bmim][$BF_4$] and acetonitrile by a refined force field. *Phys Chem Chem Phys*. 2005;7:2771–2779.
42. Lee SU, Jung J, Han YK. Molecular dynamics study of the ionic conductivity of 1-*n*-butyl-3-methylimidazolium salts as ionic liquids. *Chem Phys Lett*. 2005;406:332–340.
43. Sieffert N, Wipff G. Alkali cation extraction by calix[4]crown-6 to room-temperature ionic liquids. The effect of solvent anion and humidity investigated by molecular dynamics simulations. *J Phys Chem A*. 2006;110:1106–1117.
44. Salanne M, Simon C, Turq P. Molecular dynamics simulation of hydrogen fluoride mixtures with 1-ethyl-3-methylimidazolium fluoride: a simple model for the study of structural features. *J Phys Chem B*. 2006;110:3504–3510.
45. Micaelo NM, Baptista AM, Soares CM. Parametrization of 1-butyl-3-methylimidazolium hexafluorophosphate/nitrate ionic liquid for the GROMOS force field. *J Phys Chem B*. 2006;110:14444–14451.

46. Hertz HG, Franks F, editors. *Water, A Comprehensive Treatise*. New York: Plenum Press, 1973.
47. Dieter KM, Dymek CJ Jr, Heimer NE, Rovang JW, Wilkes JS. Ionic structure and interactions in 1-ethyl-3-methylimidazolium chloride-$AlCl_3$ molten salts. *J Am Chem Soc*. 1988;110:2722–2726.
48. Sitze MS, Schreiter ER, Patterson EV, Freeman RG. Ionic liquids based on $FeCl_3$ and $FeCl_2$. Raman scattering and ab initio calculations. *Inorg Chem*. 2001;40:2298–2304.
49. Meng Z, Dölle A, Carper WR. Gas phase model of an ionic liquid: semi-empirical and ab initio bonding and molecular structure. *J Mol Struct (THEOCHEM)*. 2002;585:119–128.
50. Turner EA, Pye CC, Singer RD. Use of ab Initio calculations toward the rational design of room temperature ionic liquids. *J Phys Chem A*. 2003;107:2277–2288.
51. Paulechka YU, Kabo GJ, Blokhin AV, Vydrov OA, Magee JW, Frenkel M. Thermodynamic properties of 1-butyl-3-methylimidazolium hexafluorophosphate in the ideal gas state. *J Chem Eng Data*. 2003;48:457–462.
52. Talaty ER, Raja S, Storhaug VJ, Dölle A, Carper WR. Raman and infrared spectra and ab initio calculations of C2-4mim imidazolium hexafluorophosphate ionic liquids. *J Phys Chem B*. 2004;108:13177–13184.
53. Hunt PA, Kirchner B, Welton T. Characterizing the electronic structure of ionic liquids: an examination of the 1-butyl-3-methylimidazolium chloride ion pair. *Chem—Eur J*. 2006;12:6762–6775.
54. Gong L, Guo W, Xiong J, Li R, Wu X, Li W. Structures and stability of ionic liquid model with imidazole and hydrogen fluorides chains: density functional theory study. *Chem Phys Lett* 2006;425:167–178.
55. Wang Y, Li H, Han S. A theoretical investigation of the interactions between water molecules and ionic liquids. *J Phys Chem B*. 2006;110:24646–24651.
56. Hunt PA, Gould IR. Structural characterization of the 1-butyl-3-methylimidazolium chloride ion pair using ab initio methods. *J Phys Chem A*. 2006;110:2269–2282.
57. Dong K, Zhang S, Wang D, Yao X. Hydrogen bonds in imidazolium ionic liquids. *J Phys Chem A*. 2006;110:9775–9782.
58. Yu G, Zhang S, Yao X, Zhang J, Dong K, Dai W, Mori R. Design of task-specific ionic liquids for capturing $CO_2$: a molecular orbital study. *Ind Eng Chem Res*. 2006;45:2875–2880.
59. Bonhôte P, Dias AP, Papageorgiou N, Kalyanasundaram K, Grätzel M. Hydrophobic, highly conductive ambient-temperature molten salts. *Inorg Chem*. 1996;35:1168–1178.
60. Nishida T, Tashiro Y, Yamamoto M. Physical and electrochemical properties of 1-alkyl-3-methylimidazolium tetrafluoroborate for electrolyte. *J Fluorine Chem*. 2003;120:135–141.
61. Shirota S, Castner EW Jr. Why are viscosities lower for ionic liquids with $-CH_2Si(CH_3)_3$ vs $-CH_2C(CH_3)_3$ substitutions on the imidazolium cations? *J Phys Chem B*. 2005;109:21576–21585.
62. Huddleston JG, Visser AE, Reichert WM, Willauer HD, Broker GA, Rogers RD. Characterization and comparison of hydrophilic and hydrophobic room temperature ionic liquids incorporating the imidazolium cation. *Green Chem*. 2001;3:156–164.
63. MacFarlane DR, Golding J, Forsyth S, Forsyth M, Deacon GB. Low viscosity ionic liquids based on organic salts of the dicyanamide anion. *Chem Commun*. 2001;1430–1431.
64. Branco LC, Rosa JN, Ramos JJM, Afonso CAM. Preparation and characterization of new room temperature ionic liquids. *Chem—Eur J*. 2002;8:3671–3677.
65. Tokuda H, Hayamizu K, Ishii K, Susan MABH, Watanabe M. Physicochemical properties and structures of room temperature ionic liquids. I. Variation of anionic species. *J Phys Chem B*. 2004;108:16593–16600.
66. Liu X, Zhang S, Zhou G, Wu G, Yuan X, Yao X. New force field for molecular simulation of guanidinium-based ionic liquids. *J Phys Chem B*. 2006;110:12062–12071.
67. Liu X, Zhou G, Zhang S, Wu G, Yu G. Molecular simulation of guanidinium-based ionic liquids. *J Phys Chem B*. 2007;111:5658–5668.
68. Zhou G, Liu X, Zhang S, He H, Yu G. A force field for molecular simulation of tetrabutylphosphonium amino acid ionic liquids. *J Phys Chem B*. 2007;111:7078–7084.
69. Yu G, Zhang S. Insight into the cation-anion interaction in 1,1,3,3-tetramethylguanidinium lactate ionic liquid. *Fluid Phase Equilib*. 2007;255:86–92.
70. Lyubartsev AP, Laaksonen AM. DynaMix—a scalable portable parallel MD simulation package for arbitrary molecular mixtures. *Comput Phys Commun*. 2000;128:565–589.
71. Tuckerman M, Berne BJ. Reversible multiple time scale molecular dynamics. *J Chem Phys*. 1992;97:1990–2001.
72. Allen MP, Tildesley DJ. *Computer Simulation of Liquids*. Oxford: Clarendon press, 1987.
73. Martyna GJ, Tuckerman ME, Tobias DJ, Klein ML. Explicit reversible integrators for extended systems dynamics. *Mol Phys*. 1996;87:1117–1157.
74. Frisch MJ, Trucks GW, Schlegel HB, Scuseria GE, Robb MA, Cheeseman JR, Montgomery JA Jr, Vreven T, Kudin KN, Burant JC, Millam JM, Iyengar SS, Tomasi J, Barone V, Mennucci B, Cossi M, Scalmani G, Rega N, Petersson GA, Nakatsuji H, Hada M, Ehara M, Toyota K, Fukuda R, Hasegawa J, Ishida M, Nakajima T, Honda Y, Kitao O, Nakai H, Klene M, Li X, Knox JE, Hratchian HP, Cross JB, Adamo C, Jaramillo J, Gomperts R, Stratmann RE, Yazyev O, Austin AJ, Cammi R, Pomelli C, Ochterski JW, Ayala PY, Morokuma K, Voth GA, Salvador P, Dannenberg JJ, Zakrzewski VG, Dapprich S, Daniels AD, Strain MC, Farkas O, Malick DK, Rabuck AD, Raghavachari K, Foresman JB, Ortiz JV, Cui Q, Baboul AG, Clifford S, Cioslowski J, Stefanov BB, Liu G, Liashenko A, Piskorz P, Komaromi I, Martin RL, Fox DJ, Keith T, Al-Laham MA, Peng CY, Nanayakkara A, Challacombe M, Gill PMW, Johnson B, Chen W, Wong MW, Gonzalez C, Pople JA. *GAUSSIAN 03 Revision C.02*. Wallingford CT: Gaussian, Inc., 2004.
75. Møller C, Plesset MS. Note on an approximation treatment for many-electron systems. *Phys Rev*. 1934;46:618–622.
76. Pople JA, Binkley JS, Seeger R. Theoretical models incorporating electron correlation. *Int J Quantum Chem Symp*. 1976;10:1–19.
77. Becke AD. Density-functional thermochemistry. III. The role of exact exchange. *J Chem Phys*. 1993;98:5648–5652.
78. Lee C, Yang W, Parr RG. Development of the Colle-Salvetti correlation-energy formula into a functional of the electron density. *Phys Rev B*. 1988;37:785–789.
79. Lopes JNC, Deschamps J, Padua AAH. Modeling ionic liquids using a systematic all-atom force field. *J Phys Chem B*. 2004;108:2038–2047.
80. Nadaf RN, Siddiqui SA, Thomas Daniel, Lahoti RJ, Srinivasan KV. Room temperature ionic liquid promoted regioselective synthesis of 2-aryl benzimidazoles, benzoxazoles and benzthiazoles under ambient conditions. *J Mol Catal A*. 2004;214:155–160.
81. Fuller, J, Carlin RT, de Long HC, Haworth DJ. Structure of 1-ethyl-3-methylimidazolium hexafluorophosphate: moldel for room temperature moleten salts. *J Chem Soc Chem Commun*.1994:299–300.
82. Noda A, Hayamizu K, Watanabe M. Pulsed-gradient spin-echo $^1H$ and $^{19}F$ NMR ionic diffusion coefficient, viscosity, and ionic conductivity of non-chloroaluminate room-temperature ionic liquids. *J Phys Chem B*. 2001;105:4603–4610.

*Manuscript received Mar. 21, 2007, and revision received Aug. 27, 2007.*